Improved intensity measures considering soil inelastic properties via multi-regression analysis

A. M. Zapata-Franco*, Y. F. Vargas-Alzate, L. G. Pujades and R. Gonzalez-Drigo

Department of Civil and Environmental Engineering, Earthquake Engineering and Structural Dynamics, Universitat Politècnica De Catalunya, Barcelona, Spain

At certain depths, the elastic properties of the ground are not affected by seismic waves. However, as they reach the surface, the soil density decreases and so does its elastic limit. This means that the expected ground motion acting at the foundation of a structure cannot be adequately described without considering the inelastic response of the soil near the surface. Therefore, one of the key elements in characterizing the seismic response of civil structures is the site effect. These depend mainly on the parameters of the soil beneath the structure and the features of the ground motion acting at the depth, where non-linear effects are negligible. Therefore, the main objective of this paper is to find an intensity measure that incorporates the information provided by the soil profile under the structure and the ground motion acting at the bedrock level. Due to the random nature of both elements, a probabilistic framework using Monte Carlo simulation has been developed to analyze this problem. For this purpose, random soil profiles have been generated to obtain a representative sample of likely scenarios of the study area. A large database of Colombian ground motion records has been used to model the seismic hazard. Finally, power functions capable of relating the input variables to the dynamic response of a large set of reinforced concrete structures have been derived by considering multi-regression analysis. It has been observed that, in several cases, intensity measures extracted from the displacement spectrum appear in the mathematical arrangements. These functions could be used to improve the efficiency of seismic risk prediction at the urban level.

KEYWORDS

soil profiles, inelastic response of soils, seismic wave propagation, Monte Carlo simulation, multi-regression analysis

1 Introduction

Soil–structure interaction is becoming fundamental in the estimation of seismic risk (Cruz and Miranda, 2021). It is because the soil beneath the structure acts as an ultimate filter that may amplify or de-amplify harmonics at specific frequencies depending on its dynamic properties. Thus, it is expected that structures having significant mass participation at specific periods may enter in resonance with the soil. One of the most remarkable examples of this effect was observed during the earthquake that affected Mexico City in 1985 (Beck and Hall, 1986). A large amplification has been

observed of long-period waves produced by a highly attenuated ground motion since the earthquake occurred far away from the site. This event shifted several conceptual paradigms on aspects related to the estimation of seismic risk. More recently, the use of advanced non-linear models considering the soil–structure interaction has provided information to better understand this complex phenomenon (Pitilakis and Petridis, 2022).

In sites of high seismic risk, and depending on the complexity (or importance) of a civil infrastructure, it is recommended to analyze its dynamic interaction with the ground by using advanced non-linear models. There are several ways to model this interaction depending on the type of foundation (Lou et al., 2011). Yet, in most cases, it is necessary to obtain a set of signals acting at the base of a soil–structure model, below which the elastic rebound theory is expected to apply (Ohnaka, 1976). These signals should be recorded on a hard rock site for the latter assumption to hold.

Therefore, a key aspect of the study of seismic risk is the characterization of the dynamic response of the soil profile (Pagliaroli et al., 2014). In this respect, it is common practice to use simplified 1D soil models to advanced 3D finite-element-method-based representations (Kaklamanos et al., 2015; Fiorentino et al., 2019). However, the higher the complexity of the model, the higher the computational time involved in solving dynamic problems. In order to tackle this computational effort, more simplified soil models are widely used. One of the most employed is the 1D model, in which the soil layers are considered Kelvin–Voigt solids (Hardin and Scott, 1967). This model is represented by a purely viscous damper and an elastic spring connected in parallel. In several cases, it allows a good approximation of the dynamic response of a soil profile. Moreover, this model has been extended to consider non-linearities associated to the loss of stiffness of the soil, and the consequent increase in damping due to shear strains (Yoshida et al., 2002).

In line with the aforementioned concept, the frequency content of the surface ground motions generated by earthquakes depends on several complex phenomena such as the type of rupture, the proximity to the epicenter and the depth, and the mechanical properties of the media through which the seismic waves pass. The variability associated with seismological parameters (i.e., rupture type, proximity to the epicenter, and depth) can be taken into account by not conditioning the selection of ground motion records to specific values. Regarding the mechanical properties of the media, depending on the depth, seismic waves may degrade the stiffness at very low shear strains (Okur and Ansal, 2007); the deeper, the lesser the stiffness degradation. Therefore, in each location, there is a depth limit in which stiffness degradation and the consequent increase in damping do not occur. Notwithstanding, close to the surface, and depending on the seismic intensity and soil type, a significant degradation of the soil properties is expected (Kostinakis et al., 2018).

Scaling ground motion records is another challenging problem in estimating seismic risk. In this respect, there are several methodologies to scale ground motions from a database. Typically, the goal is to find a significant set of records leading the structure to multiple performance levels. However, as indicated by the well-known Richter's law (Wesnousky, 1994), the number of high-magnitude earthquakes is much smaller than the number of low-magnitude earthquakes; therefore, finding high-intensity ground motion records is less probable.

Consequently, it is sometimes necessary to scale low-intensity records by significantly high factors. Therefore, scaling a single record to increased intensity values may not take into account the likely inelastic response of soils. It becomes important since some soil types modify their dynamic properties at very low shear strains. Not to mention that scaling natural ground motions to too high or too low scale factors can lead to modified records that are far from the physical properties of real ground motions (Bommer and Acevedo, 2004).

This article has been oriented to develop a computational framework for seismic risk assessment, capable of simultaneously considering in a probabilistic manner i) the main characteristics of the ground motion acting at the bedrock level; ii) the dynamic soil properties and their evolution due to the degradation caused by the seismic waves; and iii) the main features influencing the dynamic behavior of reinforced concrete frame structures. Therefore, an iterative algorithm has been designed to simulate random profiles that meet the statistical distributions of the soil properties, given a specific area. This algorithm randomizes the geometrical features used in characterizing soil profiles. It takes into account the dependency of layer thickness with depth, the correlation exhibited between closer layers, and the total length of the soil profiles.

A probabilistic set of reinforced concrete frame structures has been simulated to analyze its seismic response. Ground motion records resulting at the surface, after seismic waves had propagated through the soil model, have been used as input. The main reason for considering this structural typology is its widespread use. For instance, buildings with reinforced concrete elements are common in many earthquake-prone countries and regions (Park and Paulay, 1991). In relation to this study, buildings of this type are very common in the Andean and Caribbean regions of Colombia. In fact, this type of building is mainly found in densely populated urban areas, where there is a need to provide many housing units in a relatively small area.

It has been assumed that the simulated structures rest on a specific soil profile, which propagates seismic waves from the bedrock to the surface, by considering the equivalent linear method (Yoshida et al., 2002). The resulting seismic waves at the surface are used to perform several non-linear dynamic analyses of the structure. To do so, the city of Bogotá has been chosen as a case study. Specifically, the information regarding geotechnical studies performed over more than 20 locations within this urban area has been analyzed (FOPAE, 2011). Then, a subset of 10 locations providing information on lacustrine soil deposits was employed. In addition, a Colombian database was used to characterize the seismicity, which was provided by the "Servicio Geologico Colombiano (SGC)" (SGC, 2020).

Finally, results stemming from the following three situations were compared: i) analyzing the causal relationship between both intensity measures (IMs) extracted from the resulting ground motion that acts at the base of the building models and engineering demand parameters (EDPs) able to quantify expected damage; ii) using the ground motion records employed as input at the bedrock level to estimate IMs; iii) developing a mathematical

FIGURE 1
Schematic representation of the complete model.
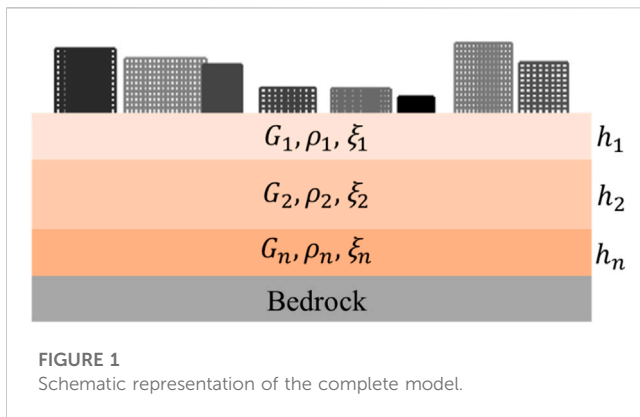
arrangement that allows combining information provided by the soil profile and the IMs calculated from the ground motion acting at the bedrock level. The results indicate that a power combination of information variables (IVs), such as those related to IMs and the soil dynamic properties, becomes an efficient intensity measure identified herein as IM_{GD}; the subscript GD stands for ground-dependent.

2 Probabilistic soil modeling

A probabilistic soil model is generally used in geotechnical applications to consider the spatial (Vanmarcke, 1977) and temporal (Carrière et al., 2018) variability of soil properties and their effects on civil structures. These models rely on statistics and probability theory to simulate soil features such as strength and stiffness, which can vary with location and time. These models estimate the uncertainties and risks associated to both the behavior of soil and the structures built on it. This helps engineers design safer and efficient structures.

Figure 1 is a sketch of the computational framework developed in this research. Input ground motions act at bedrock level. It is worth recalling that in each of the locations, there is a depth limit in which stiffness degradation and the consequent increase in damping do not occur. Below this limit, the elastic rebound theory is assumed (Ohnaka, 1976). Consequently, close to the surface, and depending on the seismic intensity (Tothong and Luco, 2007), significant degradation of soil properties is expected.

The variables represented within the soil profile scheme (shear modulus, density, damping, and layer thickness, G_i, ρ_i, ξ_i and h_i, respectively) determine its dynamic features. Due to the complex nature of soil composition, its randomness strongly influences seismic wave propagation. Moreover, at the surface level, building models are also simulated as probabilistic. Hence, the geometric and mechanical properties, as well as the gravitational loads, have been considered to be aleatory. Further details on the probabilistic generation of these variables are presented in Section 5.

All the aforementioned elements have been integrated into a probabilistic framework by following these steps:

i.   Introduce a ground motion record at bedrock level.
ii. Estimate the stiffness degradation and increase in damping of each soil layer.

iii. Calculate the resulting ground motion at the surface after propagation through the soil profile, taking into account the degradation of soil properties.
iv. The resulting ground motion estimated in the previous step acts at the base of one of the probabilistic building models.

These steps have been applied after generating samples of soil profiles and structures affected by ground motion records randomly selected from a seismic database. It is preferable that these records should have been acquired at seismic stations where the rock reaches the surface.

2.1 Case of study: Bogotá microzonation

Since 1993, the Mayor Office of Bogotá has decided to carry out seismic microzonation studies to improve design requirements for civil infrastructure (FOPAE, 2011). The objective has been two-fold: first, to better parameterize the dynamic response of the soil in front of earthquake-induced ground motions; second, to identify areas with similar seismic behavior to develop improved classification maps according to the soil type.

In accordance with the aforementioned case, a seismic response zonation map of the city was developed. The latter shows that there are six different zones, which in turn are subdivided into 16 subsets that depend on the depth of the bedrock level. This classification has considered the geotechnical description of each site, the thickness of the soil deposit, the fundamental period of the ground, and possible site effects.

In this study, calculations are performed for the lacustrine soil type, which is the most important deposit in the city. It is composed of soft clays with high compressibility, interspersed with lenses of loose sand, volcanic ash, and peat that can reach a thickness of up to 1 m. This soil type is characterized by sediment thicknesses ranging from 50 m to 500 m. In terms of dynamic properties, for lacustrine soil profiles with depths up to 200 m, the fundamental period of vibration fluctuates between 1.1 s and 2.6 s, with shear wave velocities between 140 and 280 m/s. For profiles with depths between 200 m and 300 m, the fundamental period varies from 3.5 to 3.8 s, whose wave velocities are in the range 260–290 m/s. Finally, for soil profiles that reach more than 300 m, the expected fundamental periods vary from 4.9 up to 5.8 s, with a shear wave velocity in the range 280–340 m/s. It should be noted that within the analyzed area, the lacustrine soils exhibit amplifications at high periods (between 2 s and 2.5 s) due to the effect of the soft soils and the shape of the basin in which they are located (FOPAE, 2011).

As previously stated, of the total set of analyzed locations (more than 20), 10 correspond to lacustrine deposits. Table 1 shows the number and identification (Station ID) of the stations located in lacustrine soils, as well as the main characteristics corresponding to each station, such as latitude, longitude, length of the soil deposit, number of layers into which the deposit is divided, the first three periods of the soil vibration (T_i), maximum amplitude (Max Amp.), and average shear wave velocity (Vs_{avg}). In addition, the median values ($\bar{X}$) are given in the last row of Table 1.

In the following section, the random generation process to simulate statistically compatible soil profiles, with data provided in Table 1, is explained.

TABLE 1 Summary of the main features of the lacustrine soil profile.

Soil profile	Station name	Latitude	Longitude	Length (m)	Number of layers	Fundamental period (T_i)			Max Amp	Vs_{avg} (m/s)
						T_1 (s)	T_2 (s)	T_3 (s)		
1	CBANC	4.7085	−74.0789	50	11	1.5	1.2	0.5	14.1	136
2	CEING	4.7835	−74.0459	130	19	2.8	1.1	0.4	10	186
3	CUAGR	4.7541	−74.0527	130	16	2.6	1	0.6	13	201
4	CBOG1	4.6418	−74.0803	180	21	2.6	1.2	0.4	13.3	279
5	CCORP	4.7619	−74.0937	250	21	3.6	1.5	0.9	11.6	275
6	CJABO	4.6664	−74.0993	275	21	3.8	1.7	1.1	15.1	287
7	CNINO	4.6959	−74.093	225	21	3.5	1.4	0.9	22.4	260
8	CAVIA	4.6854	−74.1188	360	21	5.3	1.8	0.9	7.5	274
9	CFLOD	4.7297	−74.1464	500	21	5.8	2.4	1.5	9.2	344
10	CTIEM	4.6943	−74.1559	425	21	4.9	1.9	0.9	11.1	345
			$\bar{X}$	237.5	21	3.55	1.45	0.9	12.3	274.5

2.2 Application of Toro's model to a lacustrine soil type

Toro et al. (Silva et al., 1996) proposed a probabilistic model for the variation of shear-wave velocity in soil and rock sites. In brief, this probabilistic model consists of three main elements: i) a model describing the random stratigraphy at the site; ii) the median wave velocity profile; and iii) a model describing the deviations of the velocity in each layer from the median, together with its correlation with respect to the layer above. In sites where there is not enough information to properly characterize uncertainties, this model appears to be an effective solution. The main elements of Toro's model, applied to the lacustrine data for Bogotá city, are described as follows.

2.2.1 Random stratigraphy at the site

For soil parameterization, the 10 lacustrine profiles specified in the aforementioned report (FOPAE, 2011) are used. The random stratigraphy is characterized by using the "Layering Model" (Silva et al., 1996). This allows considering that as the layer gets deeper, it becomes thicker. In general, this model improves the prediction of ground motion intensity at the surface by providing a better picture of stratigraphic conditions at sites with different soil types.

Hence, this model assumes that the thickness of each layer follows a depth-dependent probability distribution, where the thickness of layer i is independent of the thickness of layer i-1. The model also recognizes that soil layers tend to be thinner near the surface and thicker at greater depths (Silva et al., 1996). Accordingly, the following power law is adopted to characterize the depth-dependent rate of layer boundaries:

$$\lambda(h) = C_3 [h + C_1]^{-C_2}, \qquad (1)$$

where λ is the layer boundary rate (1/m) and h is the depth in m. The estimation of the values C_1, C_2, and C_3 is carried out by using the

capabilities of the Monte Carlo method to minimize multi-dimensional functions (Kucherenko et al., 2015).

Therefore, to estimate the probable evolution of λ, the entire number of layers composing the 10-initial set of soil profiles (193 layers) has been used; Figure 2A shows the relationship between the entire set of λ versus the median depth associated to each layer. Then, a second approach proposed in Toro (2022) has also been analyzed. It consists of running averages of λ values over a 10-m window; Figure 2B shows this relationship. After several simulations of the soil profiles, the regression obtained from the first approach was used (Figure 2A) because the resulting number of layers is more consistent with the observed information.

2.2.2 The median wave velocity profile at the site

Due to the cumulative process associated to the formation of sedimentary deposits, it has been observed that a log-normal distribution adequately parametrizes the aleatory characteristic of shear wave velocities (Toro, 2022). This parametric distribution has been adopted in the sampling process of the shear wave velocity. It should be noted that, according to Toro's model, the velocity is estimated at the layer midpoints.

Figure 3 shows wave velocity soil profiles at low shear strains ($<10^{-3}$%) for the selected locations (thinner gray lines) and their corresponding median values. Two main conclusions can be drawn from these profiles: i) the deeper, the higher the shear wave velocity; ii) the deeper, the thicker the layer, which confirms the conclusions reached in Silva et al. (1996). Both features should be considered when generating random samples of the profiles.

2.2.3 Deviations in the velocity in each layer from the median

Another important aspect observed in soil profiles is related to the spatial correlation of properties between closer layers. The closer the layers, the higher the correlation (Angelini and Heuvelink, 2018). This implies that widely separated layers tend to be less correlated.
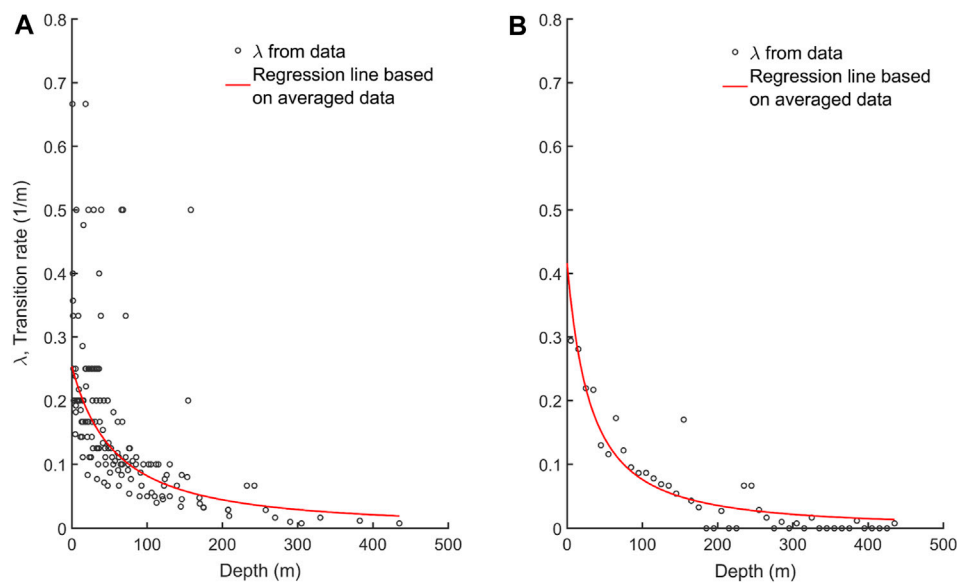
FIGURE 2
Transition rates by considering direct values **(A)** and those obtained as a running average over a 10-m window **(B)**.
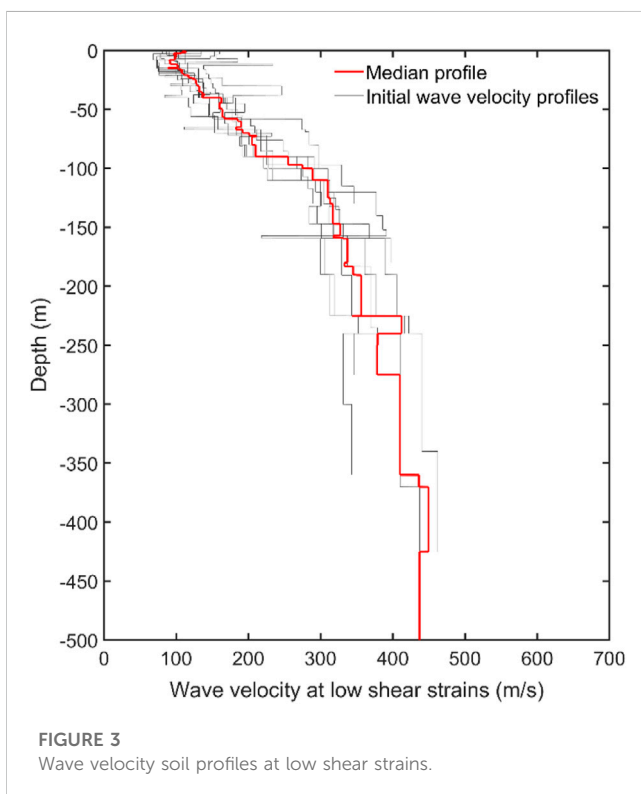
FIGURE 3
Wave velocity soil profiles at low shear strains.

$$\Psi_{i,j} = \begin{cases} i = j & \Psi_{i,j} = 1 \\ i = j \pm w & \Psi_{i,j} = 1 - \dfrac{w}{r} \geq 0 \end{cases}, \qquad (2)$$

where w is a number related to the position of a layer belonging to the same profile; r is a coefficient associated with the rate of correlation between adjacent layers. In this research, r has been fixed to 100/3.

2.3 Probabilistic generation of soil profiles based on the Monte Carlo simulation

The Monte Carlo simulation can be applied to solve a large variety of numerical problems (Kroese and Rubinstein, 2012). It is mostly used as a tool to assess the uncertainty in complex models and systems. It can be seen as a numerical technique to generate random datasets for assessing uncertainty in a system. Accordingly, for each variable, random datasets are generated by assuming parametric statistical distributions that fit the conditions of the study. This simulation technique also makes it possible to develop a mathematical arrangement that includes variables that influence the model. Based on the description of the probabilistic features that must meet the soil profiles, their statistical realizations have been obtained via Monte Carlo simulations. Figures 4A, B show the random set of 1,000 shear wave velocity soil profiles that have been employed in the development of the probabilistic framework proposed in this research. It is worth mentioning that these soil profiles correspond to low shear strains.

The damping properties at low shear strains have been obtained by using degrading curves for the soil type analyzed. This is discussed further in Section 4 of this article. Another important variable influencing the dynamic properties of the simulated soil profiles is density. This has been indirectly considered a random

In order to consider the likely correlation exhibited by the shear wave velocity between closer layers, it is necessary to employ a correlation hypothesis (Vargas–Alzate et al., 2018). It has been assumed that the correlation between adjacent soil layers ($\psi_{i,j}$) decreases with distance by means of the following model

FIGURE 4
Probabilistic soil profiles for shear wave velocity and damping. **(A,B)** Soil profiles at low shear strains. **(C,D)** Degraded soil profiles.

FIGURE 5
(A) Probabilistic soil profiles for density. **(B)** Relationship between elastic vs elongated periods.

variable by using the following relationship proposed in Nakamura (1989):

$$\gamma = 8.32 \cdot log_{10} Vs - 1.61 \cdot log_{10} H, \qquad (3)$$

where H stands for depth in m, Vs represents shear wave velocity (m/s), and γ is the unit weight (kN/m³). Figure 5A depicts the random set of density profiles after applying Equation 3. Figure 5B relates the elastic periods with the elongated ones. The latter is further discussed in Section 4.

3 Seismic hazard characterization

A seismic hazard is defined as the potential for future earthquakes at a given site (Shedlock, 2002). This hazard is usually expressed in terms of acceleration and the probability that a certain level of ground motion is exceeded within a given period of time. Seismic hazards can be estimated using several methods, including probabilistic seismic hazard analysis (PSHA) and deterministic seismic hazard analysis (DSHA) (Krinitzsky, 2003). Accurate seismic hazard characterization is essential for several reasons, including risk assessment, effective planning, and informed decision-making, to prevent potential earthquake-related risks. In addition, accurate seismic hazard characterization can lead to the development of a resilient civil infrastructure that can better withstand seismic events.

3.1 Colombian seismic database

Colombia is located on the Pacific Ring of Fire, an area with the highest concentration of earthquakes in the world (Comartin et al., 2000). The country lies at the intersection of three tectonic plates: the Caribbean, the South American, and the Nazca plates. This geological feature significantly increases the seismic risk in Colombia when compared to other regions. The main source of seismicity is related to the subduction zone of the Colombian Pacific plate and to the geological faults caused by the convergence of the three plates. Studies show that almost 83% of the population lives in moderate-to-high seismic risk areas.

In terms of geographical configuration, Colombia has been divided into five regions. The city of Bogotá is located in the central region, which is the most densely populated and economically active in the country. It includes the central, eastern, and western mountain ranges, running from southwest to northeast, and covers approximately 2,825,540 km², or 30% of Colombia's territory, with a population density of 121.82 inhabitants/km².

Ground motions recorded in Colombia between 1993 and 2017 have been compiled, with a magnitude greater than 4.0 Mw. Accordingly, a total of 1992 records have been extracted from the SGC (2020). They have been divided into two groups based on the ground conditions in which they were recorded. The first category includes signals recorded on rock, with a total of 1,236 records. The second group includes signals recorded on less rigid ground, with a total of 756 records. In both cases, environmental noise and other factors that could affect the accuracy of the signal have been corrected. It is worth recalling

FIGURE 6
Seismic stations around Bogota city.

that the elastic rebound theory applies below the bedrock level (see Figure 1). This implies that linear scaling of ground motions below this limit can be accepted without excessive error. Therefore, it seems logical to use the outcrop datasets as input at the base of the soil model (see Figure 1).

3.2 Ground motion selection based on a proximity algorithm

In order to obtain a more precise representation of the seismogenic environment of Bogotá, an algorithm has been developed to identify the seismic records acquired at the stations closest to a study point within the Colombian territory. It starts by taking the entire set of 1992 ground motions and collecting the relevant information, such as date of the seismic event, magnitude, station name, and epicentral and hypocentral distance. Then, based on the coordinates of the studied area and the maximum radius around this point, the nearest stations are identified and the signals recorded are extracted and addressed to two folders depending on whether the station is located on soil or on rock. In parallel, a map that allows identifying the analyzed point, and the stations delimited within the radius, is created. Moreover, the program provides the acceleration, velocity, and displacement spectra.

For this study, Bogotá city (latitude 4.6097 and longitude −74.0817) has been used as a reference point by considering a radius of 400 km. Thus, using the aforementioned algorithm, a set of 1,023 ground motions recorded on rock have been identified.

Figure 6 shows both the study point and the nearest stations. Table 2 shows the distances and IDs of the nearest stations found within a radius of 400 km around Bogotá.
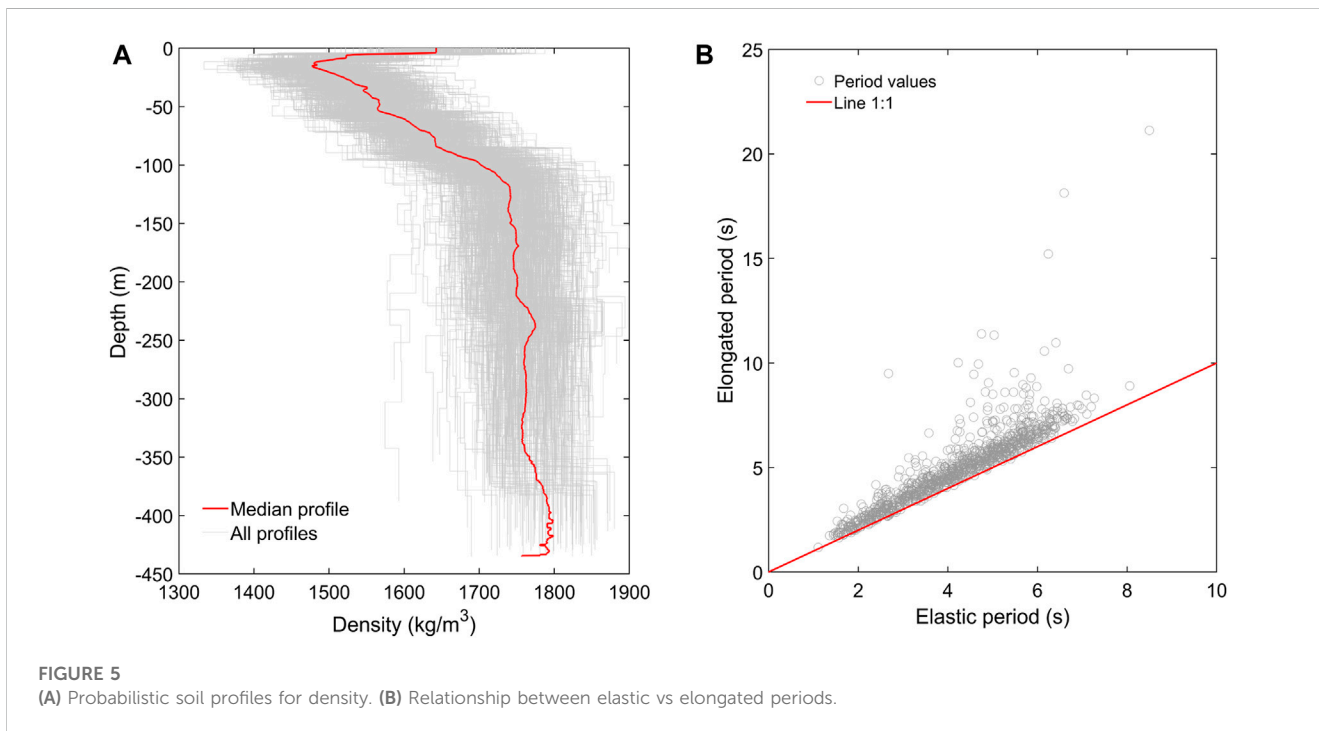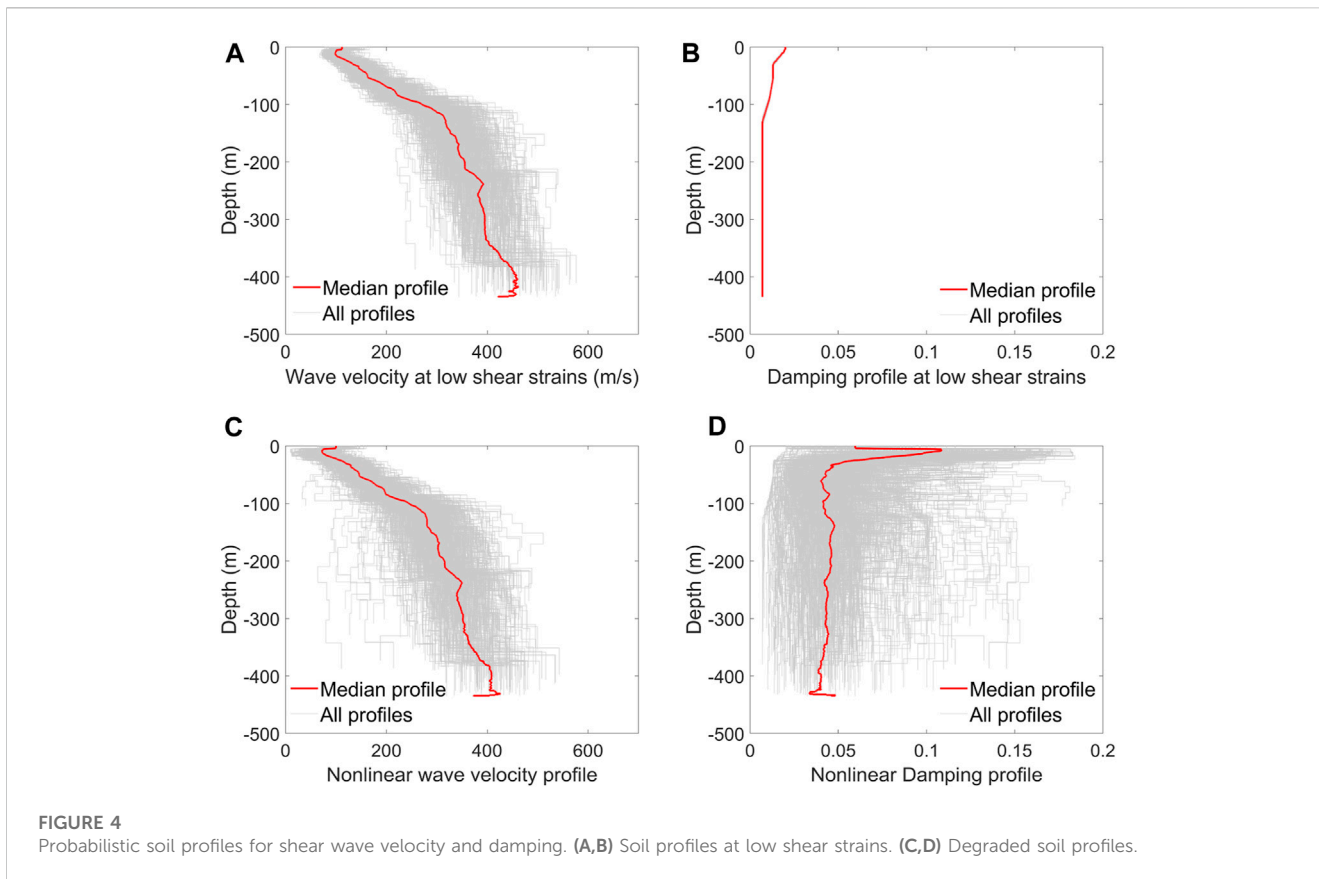
TABLE 2 Lists of the stations that were found within a radius of 400 km of the study site.

Distance (km)	ID station	Distance (km)	ID station	Distance (km)	ID station	Distance (km)	ID station	Distance (km)	ID station
1.54	CTEJE	26.83	CCAQ1	164.66	MHOSP	241.86	CBARI	301.05	CCAL2
2.29	CCKEN	27.66	CCAQ2	167.88	CMAN1	242.01	CTULU	301.12	CBUIS
2.47	CBART	37.48	CROSA	168.73	MCOLO	248.17	CTOCH	302.47	RAC06
2.6	CBOG2	39.69	CQUET	171.64	CCALA	252.12	CTRUJ	303.26	RAC05
3.49	CBOG1	41.29	CQUE2	174.17	CSTRC	256.92	CBET2	304.37	RAC02
3.56	CPGA1	41.59	CCHIN	174.34	CBOCA	259.53	CBETA	304.58	CCAL7
3.88	CREAC	48.37	CANAP	174.97	CSUES	260.41	CYOTO	304.85	RAC03
4.07	CVITE	55.89	CARBE	175.05	CARME	275.26	CMACA	305.76	CCAL8
4.64	CUNMA	68.97	CVIL1	175.05	CPOST	280.65	CSJGU	307.98	CCAL3
5.27	CARAN	70.08	CCNEG	178.49	CMAZP	280.67	CBARR	307.99	RAC04
6.29	CGRAL	76.12	CGUAD	181.1	CNOBS	283.84	RAC01	309.68	CDAGU
6.54	CJABO	102.95	CFQNE	181.51	CFILA	286.51	CECAL	317.65	CGARZ
8.43	CARTI	124.2	CIBA3	181.76	CSLUI	287.58	CGIR2	319.76	CPLAT
8.97	CFONT	124.25	CVHER	182.83	CSONS	288.11	CBUC5	324.75	CTAME
9.05	CCARV	129.1	CIBA1	182.9	CPER2	290.85	CBUC4	344.04	CPAM3
9.68	CNINO	130.71	CPRAD	185.18	CPER3	291	CGIRO	345.37	CSAL1
10.56	CSMOR	130.99	CIBA2	193.32	CGENO	294.06	CBUC6	346.89	CPAMP
10.93	CBANC	131.61	CTUN2	196.32	CPER1	294.68	RAC10	352.08	CPAM2
11.65	CMARI	132.16	CTUN3	201.6	CRIO2	295.08	CBUC2	356.48	CDABE
11.99	CUSAQ	133.51	CTUN1	202.64	CRIOS	295.53	CBUCF	362.88	CPOP3
12.04	CTVCA	137.24	CNOCA	202.96	CYOPA	295.6	CBUC1	365.08	CPOP5
12.23	CBOSA	138.48	CNORC	205.32	CANSE	296.1	RAC09	366.75	CBMAL
12.4	CTIEM	146.1	CRECR	209.89	CPLA1	296.48	RAC08	367.47	CPOP2
12.56	CTUNA	147.91	CPENS	216.94	CVICT	297.74	RAC11	372.56	CPOP1
14.2	CPSUB	152.36	CORTC	218.59	CPBER	297.98	CCAL5	379.01	CFLOR
15.05	CFLOD	155.74	MEMTE	227.9	CNEIV	300.36	CSAMU	384.45	CSJUR
16.43	CUAGR	158.47	CCOLO	232.65	CANDE	300.71	CTUTU	390.25	CSAGU
16.88	CCORP	163.69	MUNAL	233.24	CSVIC	300.74	CCAL4		
17.3	CUSAL	163.98	CPALE	234.53	CROLD	300.82	RAC07		
19.69	CEING	164.01	MPALE	235.69	CVERS	300.89	CPTEJ		

3.3 Ground motion scaling

There are several methods for selecting ground motions from a database (Haselton et al., 2012). Typically, the aim is to have enough records leading the structure to different performance levels. However, in current databases, there are often no strong ground motion records with high intensity values. This can cause excessive scaling, which may introduce bias in the structural response (Haselton et al., 2012). To address this issue when using cloud analysis (Jalayer et al., 2015), the method proposed by Vargas–Alzate et al. (2022b) to select and scale ground motion records has been used.

i. Identify the database.

ii. Identify the IM for selecting and scaling records.

iii. Calculate the IM for each ground motion in the dataset.

iv. Sort the ground motion records in descending order based on the calculated IM values.

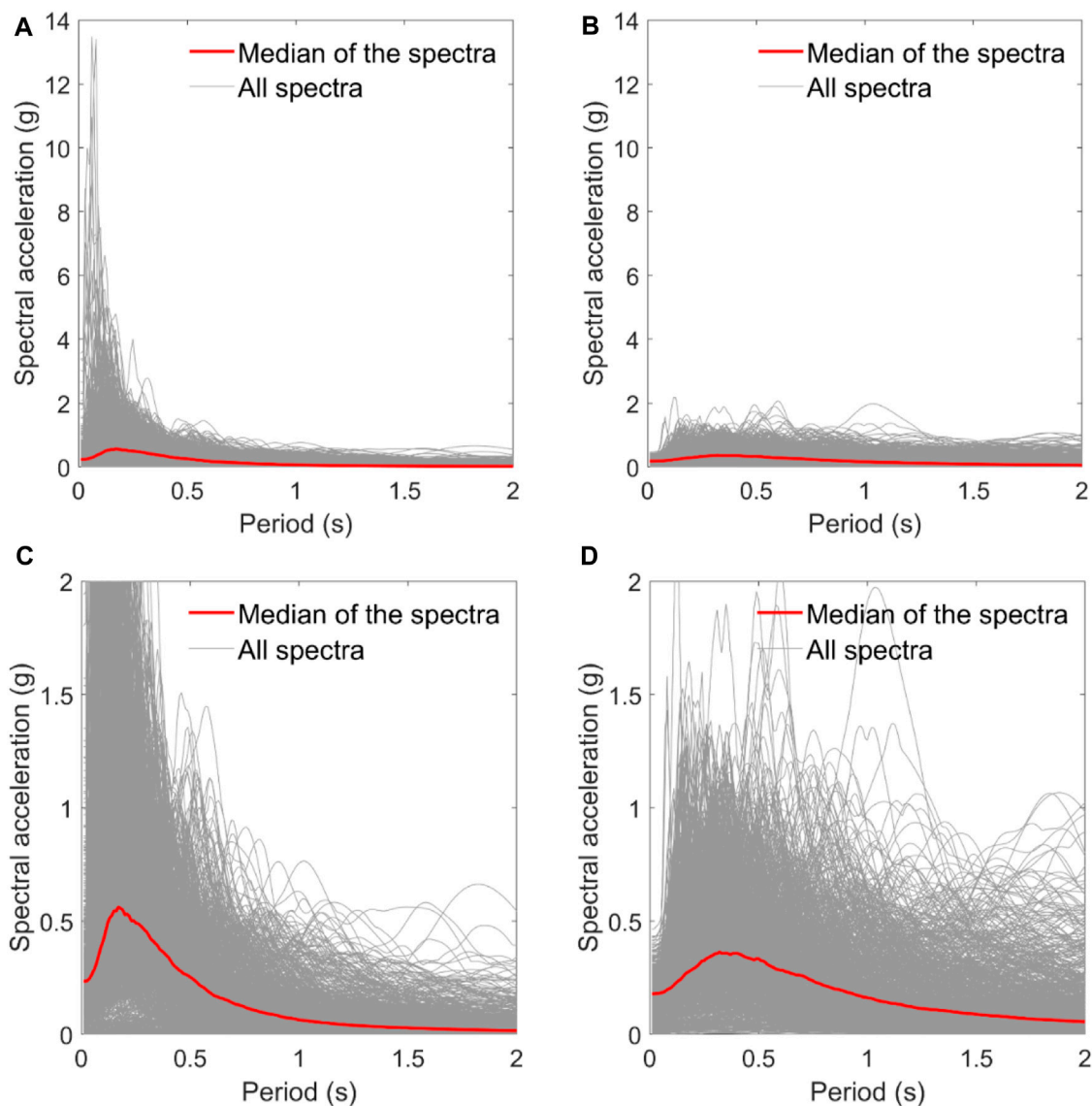v. Define both the intensity intervals for scaling and the number of records per interval.

FIGURE 7
(A) Spectra of ground motion records acting at bedrock level. **(B)** Spectra of the resulting ground motions at the surface after the propagation process. **(C,D)** Close-up of the spectral acceleration below 2 g.

vi. Scale the first ranked ground motion record so that the IM value falls into the highest interval. Calculate the scale factor so that the IM values are uniformly distributed within the interval. If the IM fulfills the interval condition, no scaling factor is considered. Repeat the process until there are N_{rec} records in the highest interval.

vii. Repeat the previous steps to have the desired number of ground motion records in each interval.

The choice of an optimal IM for this article mainly depends on its efficiency. In this regard, Sa (T1), the spectral acceleration at the fundamental period, is one of the most frequent IMs. However, its ability to explain the non-linear dynamic response of systems has been questioned (Grigoriu, 2016; Luco and Cornell, 2019). Instead, an IM based on the geometric mean of spectral acceleration values

estimated at periods covering both higher and elongated modes of response, Sa_{avg}, is more efficient than Sa (T1) (Eads et al., 2015; Kazantzi and Vamvatsikos, 2015). Analogously, an IM identified as *AvSa* is used here to select and scale the datasets. It should be noted that *AvSa* differs from Sa_{avg}, in that it is calculated using the arithmetic mean rather than the geometric one.

The period range for averaging the spectral ordinates of *AvSa* should be determined from the dynamic properties of the entire building population (Kohrangi et al., 2017). This range has been set at (0.1–1.8) sec, which contains the fundamental periods of the generated models, as can be seen in Vargas–Alzate et al. (2022b). The intensity levels defining the upper and lower limits of each band (step v) range from 0.04 to 0.4 g at 0.04 g intervals (i.e., 10 bands have been defined). Therefore, the horizontal components of 1,000 ground motion records (100 per band) have been obtained from the seismic

database. It should be noted that the scaling is applied to the ground motion records acting at the bedrock level.

Figure 7A shows the spectra of the selected and scaled ground motion records, and it can be seen that the spectral acceleration values at low periods are by far unexpected. In this regard, it is worth mentioning that these structures have been developed so that they meet the performance levels of a high-seismic hazard region (Vargas–Alzate et al., 2022b).

In order to fully explore the inelastic response of the analyzed set of structures, the intensity of some ground motion records should be increased by using high scale factors. For instance, it is necessary to scale some ground motion records until the *PGA* values are in the order of 4 g, which can be seen as improbable according to observed seismicity. Yet, by only considering these high intensity values, it is possible to properly derive fragility functions.

In line with the aforementioned concept, it should be noted that the window of periods in which the intensity measure is calculated includes high abscissa (i.e., higher than 1 s). This causes the resulting average intensity values (*AvSa*) to be much lower than the peak ordinate in the corresponding spectrum. This effect is more notorious when considering records acquired in stiff soil, as in the current study, which exhibit large amplifications at low period values. Consequently, very small displacements in the structures are expected. Moreover, these high spectral ordinates are observed within the ground motions acting at the bedrock level, as can be seen in Figure 7A. Since a soil profile acts as a filter, and in the current study it attenuates low period values due to the stiffness of the lacustrine soil, it should be noted that the resulting spectral ordinates at the surface (see Figure 7B) agree with realistic values.

4 Seismic wave propagation by considering a 1D model

One-dimensional site response analysis is associated with vertically propagating shear waves through horizontally layered media. To account for material damping, the soil layer is modeled as a Kelvin–Voigt solid. This is a material whose resistance to shearing deformation is the summation of the elastic and viscous parts (Kumar and Mondal, 2017). Numerically, site response analysis based on 1D models can be performed using linear, equivalent linear, and non-linear methodologies. Among them, the equivalent linear method is widely followed because of its simplicity and reasonable accuracy with respect to non-linear-based results (Yoshida et al., 2002). This methodology has been used here to assess the stiffness degradation and the consequent increase in damping within the soil profile.

At present, there are numerous software programs and codes that can perform site response analysis following 1D models. In this article, the WaveProp code (Pitilakis, 2023) has been used as a solver to develop the iterative procedure related to the equivalent linear method. In addition, due to the low computational time that this method consumes, it becomes an ideal candidate to consider the uncertainties in the mechanical properties of the materials. Hence, this method has been used with a twofold objective: i) account for uncertainties in the mechanical properties of soils; ii) provide an estimate of the modified properties of soil layers affected by seismic waves.

As described previously, the propagation of the seismic waves produces the degradation of soil stiffness and, consequently, the

increase of material damping in each layer. These changes depend on the maximum shear strain reached during a seismic event. There are several methods to consider this effect. One of the most commonly used is the equivalent linear method (Kumar and Mondal, 2017). This method consists of estimating, from iterative linear approximations, the physical properties of an analogous soil profile whose dynamic response is similar to that obtained by an exhaustive but computationally expensive method, such as non-linear dynamic analysis. These calculations are performed in the frequency domain, which substantially reduces the computational effort.

In the equivalent linear method, the degradation of the stiffness and the consequent increase in the damping of the material in each layer are considered using the normalized shear modulus (G_0/G_{max}) and hysteretic damping curves, both as a function of the maximum shear strain reached during the dynamic process. For the case study, the reference curves have been selected from the geotechnical report described previously (FOPAE, 2011). Figure 8 shows the stiffness degradation (A) and damping curves (B) used in this study.

The iterative process associated to the equivalent linear approximation is described step by step as follows.

i. Initially, each soil layer is modeled considering initial stiffness (G_0) and damping values (ξ_0) corresponding to low shear strains (see Figures 4A, B)

ii. From the properties described in the previous step, the time-history of shear strains in each soil layer is calculated, $\gamma(t)$; this has been obtained using a one-dimensional soil model

iii. From the maximum strain reached during the propagation, $\gamma_{max} = \max{(|\gamma(t)|)}$, the effective strain in each layer is estimated as $\gamma_{eff} = \alpha^\star \gamma_{max}$; in this research, $\alpha = 0.65$

iv. For each layer, a new pair of G_i and ξ_i values is obtained from the degrading curves for stiffness and damping (see Figure 8)

v. Steps ii to iv are repeated until the difference between two consecutive values of G and ξ is less than 1%

vi. From the final values of G and ξ, for each soil layer, a linear site response analysis can be performed

This iterative procedure has been used to estimate the non-linear response of the probabilistic soil profiles shown in Figures 4A, B. It should be noted that the density values (see Figure 5A) are used to estimate *Vs* from the resulting *G* values. Thus, Figures 4C, D show the resulting soil profiles after performing the equivalent linear approximation. Finally, Figure 5B compares the elastic versus the elongated periods. In all cases, a stiffness degradation of the soil profile has occurred. It should be noted that there are several outliers, which indicate that the equivalent linear method has not been able to achieve convergence. This is probably because the maximum shear strain reached the ultimate value shown in Figure 8. It has been estimated that the number of profiles meeting this condition is 122.

5 Probabilistic structural modeling

The development of accurate building models depends on the amount of information about the mechanical and geometric properties of structural components (Vargas–Alzate et al., 2022b).
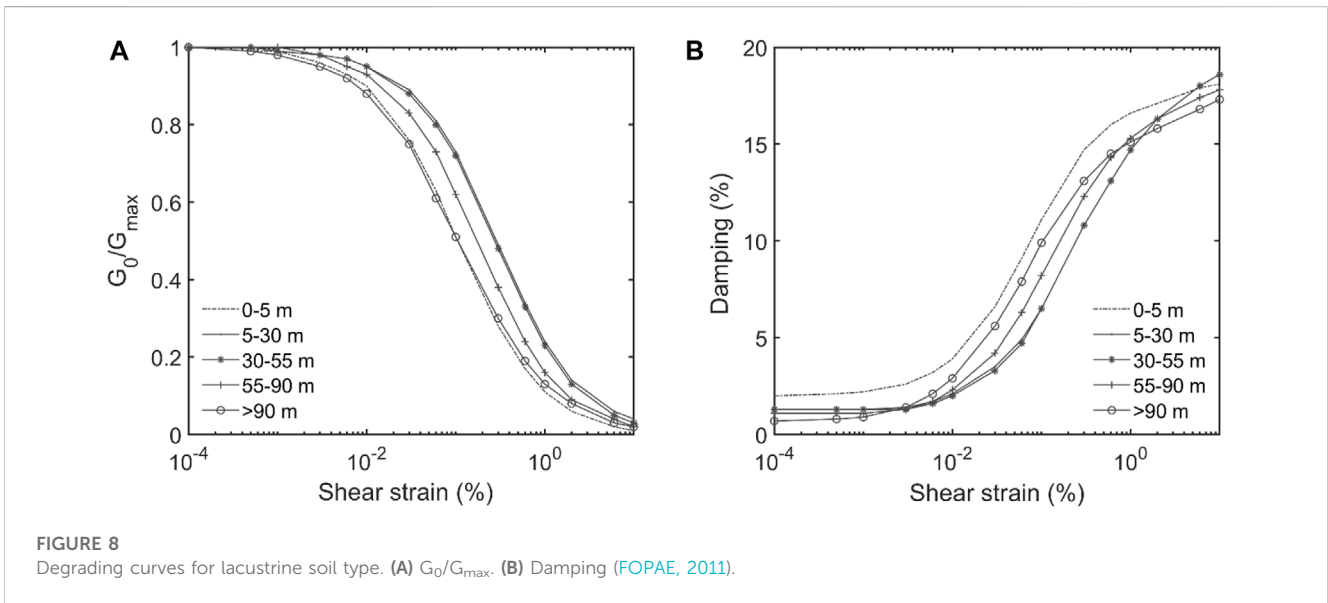
FIGURE 8
Degrading curves for lacustrine soil type. **(A)** G_0/G_{max}. **(B)** Damping (FOPAE, 2011).

TABLE 3 Mean values, μ; standard deviations, σ; and coefficient of variation, c.o.v., of the assumed random variables.

	RC frames		
	μ (kPa)	σ (kPa)	c.o.v
LL	1	0.1	0.1
DL	4.5	0.18	0.04
Fc	2.5E4	2.5E3	0.1
Fy	4.6E6	2.3E5	0.05
Ec	2.3E7	1.84E6	0.08
Es	2.18E8	1.09E7	0.05

FIGURE 9
One hundred building samples generated according to the approach developed in Vargas−Alzate et al. (2022b).

In urban contexts, knowledge of the spatial distribution of several physical properties is also of importance. Basic information should include the number of structures belonging to specific typologies, the distribution of building height and length, number of stories, and spans. Hence, the number of stories, N_{st}; the number of spans, N_{sp}; story height, H_{st}; and span length, S_l, are considered random. N_{st} and N_{sp} follow a uniform discrete distribution in the intervals (3, 13) and (3, 6), respectively; H_{st} and S_l are distributed uniformly in the interval (2.8, 3.2) m and (4, 6) m, respectively.

Data on the variability of the mechanical and geometric properties of the structural elements and those of the applied loads are also useful. Accordingly, random variables such as the concrete compressive strength, fc; the elastic modulus of the concrete, Ec; the steel yielding, fy; the elastic modulus of the steel, Es; live loads, LL; and permanent loads, DL, are assumed as continuous Gaussian distributions. It is worth noting that live loads are assigned as a fraction (33%) of the design value (Eurocode 8). Table 3 shows the statistical moments of these variables.

In order to assign the cross-section dimensions of the first story columns, the following equation has been used.

$$W_c \text{ or } D_c = c_1 * \ln(N_{st}) + c_2 * S_l + c_3 * \Phi_{1,0} + c_4, \qquad (4)$$
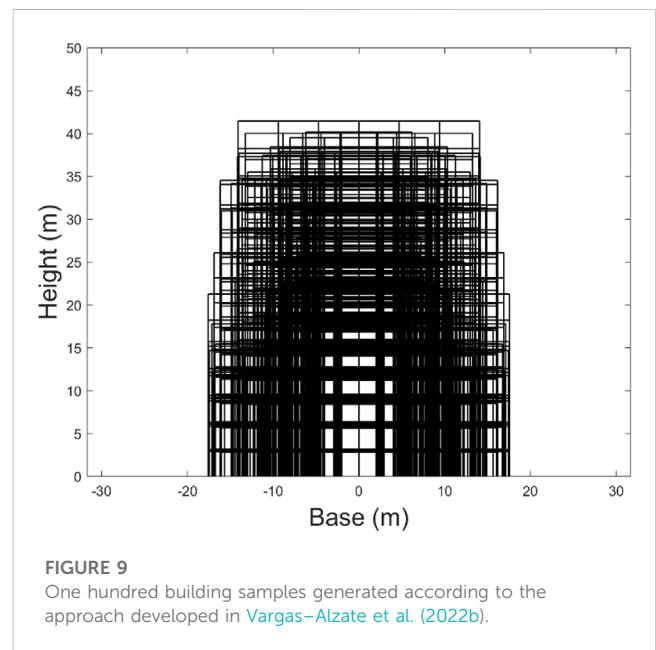
where c_i are coefficients that may be adjusted depending on the data distribution of the analyzed area. For this study, $c_1 = 0.4$, $c_2 = 0.05$, $c_3 = 0.01$, and $c_4 = -0.35$; $\Phi_{1,0}$ represents the standard normal distribution. It should be noted that columns are not necessarily square, that is, one random sample is generated for the width, W_c, and one for the depth, D_c, of the element (Eq. 4). For upper stories, the size of columns decreases systematically by 5 cm for every three stories. Values generated are rounded to the nearest multiple of 5 cm to be consistent with the real dimensions of RC elements.

The width of beams, W_b, depends on the number of stories of the building model and on the span length, and it has been calculated using the following equation:

$$W_b = b_1{}^*N_{st} + b_2{}^*S_l + b_3, \tag{5}$$

where b_i are coefficients that depend on the characteristics of the study zone. For the hypothetical case study, $b_1 = 0.01$, $b_2 = 0.02$, and $b_3 = 0.19$. The depth of the beams, D_b, is obtained using the following equation:

$$D_b = g_1{}^*N_{st} + g_2{}^*S_l + g_3, \tag{6}$$

where $g_1 = 0.01$, $g_2 = 0.05$, and $g_3 = 0.17$. No random term is considered for beams. Accordingly, 1,000 probabilistic samples of buildings have been generated to randomly pair with the soil profiles shown in Figure 4; Figure 9 shows 100 cases from all the structural models generated.

6 Intensity measures and engineering demand parameters

For a dataset of ground motion records, a basic mathematical background along with proper numerical tools allow extracting some variables representing the seismicity of an area. In the context of earthquake engineering, such variables are known as instrumental IMs. Ideally, an IM should contain enough information about the earthquake, so according to it, the structural response can be predicted with confidence (Pejovic and

Jankovic, 2015). Notice that an IM can depend either on the ground motion record or on both the ground motion and structural features (Eads et al., 2015). In this article, information related to the soil properties arises to increase the efficiency of the IMs.

6.1 Intensity measures

Three types of IMs have been considered in this research. The first type corresponds to IMs derived from the dynamic equilibrium equation for single-degree of freedom (SDoF) systems.

$$m\ddot{u}(t) + c\dot{u}(t) + ku(t) = -m\ddot{u}_g(t), \tag{7}$$

where $\ddot{u}(t)$, $\dot{u}(t)$, and $u(t)$ are the spectral acceleration, velocity, and displacement time history responses of the SDoF, respectively; $\ddot{u}_g(t)$ is the acceleration ground motion; m, c, and k represent the mass, damping, and stiffness of the system, respectively. IMs from 1 to 6 belong to this category (see Table 4). The second type of IMs is extracted from the equivalent velocity spectrum (Benavent-Climent et al., 2004; Yazgan, 2012; Cheng et al., 2015; Güllü et al., 2019). IMs 7 and 8 belong to this category (see Table 4). Finally, the third type of IMs is calculated from the record. It means no spectral calculations are performed to obtain these IMs. IMs 9 to 16 are of this type (see Table 4).

TABLE 4 Intensity measure description.

IM number	Formula	Intensity measure
1	$Sa(T) = max(\|\ddot{u}_g(t) + \ddot{u}(t,\xi,T_1)\|)$	Spectral acceleration at T_1
2	$Sv(T) = max(\|\dot{u}(t,\xi,T_1)\|)$	Spectral velocity at T_1
3	$Sd(T) = max(\|u(t,\xi,T_1)\|)$	Spectral displacement at T_1
4	$AvSa = \frac{\sum_{i=1}^{n} Sa(T_i)}{n}$	Average spectral acceleration
5	$AvSv = \frac{\sum_{i=1}^{n} Sv(T_i)}{n}$	Average spectral velocity
6	$AvSd = \frac{\sum_{i=1}^{n} Sd(T_i)}{n}$	Average spectral displacement
7	$VE(T) = \sqrt{2E_I(T_1)}$	Equivalent velocity at T_1
8	$AvVE = \frac{\sum_{i=1}^{n} VE(T_i)}{n}$	Average equivalent velocity
9	$PGA = max(\|\ddot{u}_g(t)\|)$	Peak ground acceleration
10	$PGV = max(\|\dot{u}_g(t)\|)$	Peak ground velocity
11	$PGD = max(\|u_g(t)\|)$	Peak ground displacement
12	$SED = \frac{\pi}{2g} \int_{t_{5\%}}^{t_{95\%}} \ddot{u}_g(t)^2 \, dt$	Specific energy density (Sarma, 1971; Sarma and Yang, 1987)
13	$I_A = \sqrt{\frac{1}{\Delta} \int_{t_{5\%}}^{t_{95\%}} \ddot{u}_g(t)^2 \, dt}$	Arias intensity (Arias, 1970)
14	$I_C = \sqrt{\frac{1}{\Delta} \int_{t_{5\%}}^{t_{95\%}} \dot{u}_g(t)^2 \, dt}$	Characteristic intensity (Reed and Kassawara, 1990)
15	$vel_{RMS} = \int_{t_{5\%}}^{t_{95\%}} \dot{u}_g(t)^2 \, dt$	Root mean of the velocity
16	$acc_{RMS} = \int_{t_i}^{t_f} \|\ddot{u}_g(t)\| \, dt$	Root mean of the acceleration (Housner, 1975)
17	$CAV = acc_{RMS}{}^{1.5} \sqrt{\Delta}$	Cumulative absolute velocity (Park et al., 1987)
18	$I_F = PGV^*\Delta^{0.25}$	Fajfar intensity (Fajfar et al., 1990; Pinzón et al., 2020)

6.2 Engineering demand parameters

EDPs are used to design or assess the expected behavior of buildings. Their most valuable feature is that they provide the best possible quantification of the level of performance of structures that are subjected to the ground motions induced by earthquakes. One of the most used EDPs for estimating this level is the maximum inter-story drift ratio, MIDR (Mayes, 1995). This EDP is highly used in both designing and assessing the vulnerability of buildings.

For a story i, the evolution of the inter-story drift is given by

$$IDR_{i,n}(t) = \frac{\delta_{i,n}(t) - \delta_{i-1,n}(t)}{h_i}, \qquad (8)$$

where $\delta_{i,n}(t)$ is the displacement at the floor i of the structure; h_i represents the height of the story i. The maximum inter-story drift ratio at the story i, $MIDR_i$, can be calculated as follows:

$$MIDR_i = max\left(\sqrt{IDR_{i,x}^2(t) + IDR_{i,y}^2(t)} \right), \qquad (9)$$

In order to estimate the damage level of the most affected story, the maximum inter-story drift ratio observed in the building, MIDR, is given by

$$MIDR = max\left[MIDR_1, MIDR_2 \dots MIDR_{N_{st}} \right]. \qquad (10)$$

Based on Equation 10, this EDP has been employed in this research to estimate the expected performance of the simulated structures.

7 Statistical analysis of IM-EDP clouds

There are many numerical methods to simulate the non-linear dynamic response of buildings. They range from adapted linear-static-based methods to more advanced ones, considering the non-linear static (pushover-based methods) or dynamic response of a structure (non-linear dynamic analysis, NLDA). The latter has been employed in this research since it is the most reliable numerical tool to simulate the non-linear dynamic response of buildings.

Once defined and characterized hazard (see Section 3) and exposure (see Section 5), 1,000 NLDAs are performed. The Ruaumoko software has been used to perform structural analyses (Carr, 2007). After performing these analyses, it has been found that there are several simulations in which the capacity of the structure to withstand gravity loads is exceeded; in other words, the model is indicating structural collapse. These results must be excluded from the statistical analysis as they are excessively governed by chaos. Collapses have been identified as simulations providing a Park–Ang damage index higher than 1 (Park et al., 1987). This criterion is very efficient in detecting structural collapses in the current research. In addition, profiles whose elongated periods indicated lack of convergence in the equivalent linear method have also been excluded. Accordingly, 670 out of the 1,000 generated samples have been used to perform the statistical analysis. The resulting cloud of IM-EDP points is then employed to analyze some statistical properties related to data variability.

7.1 Efficiency

In this study, IM-EDP relationships are characterized by performing a non-linear regression analysis in the log–log space. In this sense, the following general linear least-square model allows several types of non-linear regressions:

$$y = \alpha_0 + \sum_{i=1}^{N_{IV}} \sum_{j=1}^{n} \alpha_{j+(i-1)*n} z_j + \varepsilon, \qquad (11)$$

where N_{IV} represents the number of information variables (IV) considered in the regression model; n represents the polynomial degree; $\alpha_0, \alpha_1, \dots \alpha_{N_{IV}*n}$ are the scalars maximizing the coefficient of determination, R^2, between the model and data; z_j represents basic functions; and ε represents the residuals. It can easily be seen how a polynomial regression falls within this model. That is, $z_1 = x, z_2 = x^2 \dots z_n = x^n$. Substituting in Eq. 11 $y = \ln EDP$ and $z_j = (\ln IV_i)^j$, the general linear least-squares model using polynomial functions can be used to extract statistical information from IM-EDP pairs according to the following equation:

$$\ln EDP = \alpha_0 + \sum_{i=1}^{N_{IV}} \sum_{j=1}^{n} \alpha_{j+(i-1)*n} (\ln IV_i)^j + \varepsilon. \qquad (12)$$

This equation allows multi-linear ($n = 1$) and -quadratic ($n = 2$) regression models in the log–log space. In this way, several sources of information can be considered simultaneously to better predict a specific EDP. R^2 has been used herein to provide an estimation of the variability when analyzing IM–EDP pairs. That is, the higher the R^2, the lower the variability when predicting some EDP, given an IM. Consequently, the IM providing the highest R^2 is the most efficient one. Further information regarding the development and implementation of this type of polynomial model in the log–log space can be found in Chapra (2018).

7.2 Cloud analysis

Cloud analysis requires calculating the best-fit curve between a set of IM–EDP realizations in the log–log space. The resultant curve is used to estimate the median of a parametric statistical distribution, given an IM value. The variability of this parametric distribution is estimated as the logarithmic standard deviation of the regression ($S_{y/x}$). In this way, the probability of exceeding a certain damage threshold given an IM value can be calculated. Variables described in Section 6 are used as IMs as follows, and MIDR is used as an EDP. R^2 has been calculated considering three approaches: i) estimating IMs from the ground motion acting at the base of the structure; ii) using the ground motion records acting at bedrock level to estimate IMs; iii) developing a multi-regression model that allows combining information provided by the soil profile and the IMs calculated in the previous approach. Two types of polynomials have been used to calculate R^2. It means $n = 1$ and $n = 2$ have been replaced in Equation 12, thus providing two new coefficients of determination, R_L^2 and R_{NL}^2, where the subscript L stands for linear and NL for non-linear.

7.2.1 Approach 1: IM−EDP pairs using ground motions acting at the base of the buildings

In this case, IMs have been calculated by using the resulting ground motions at the surface once the seismic waves pass and degrade the soil profile properties. In this way, Figure 10 shows the bivariate distribution between IMs and MIDR. From this figure, it can be seen that several IMs, especially those related to velocity and displacement quantities, exhibit high efficiency. This result is
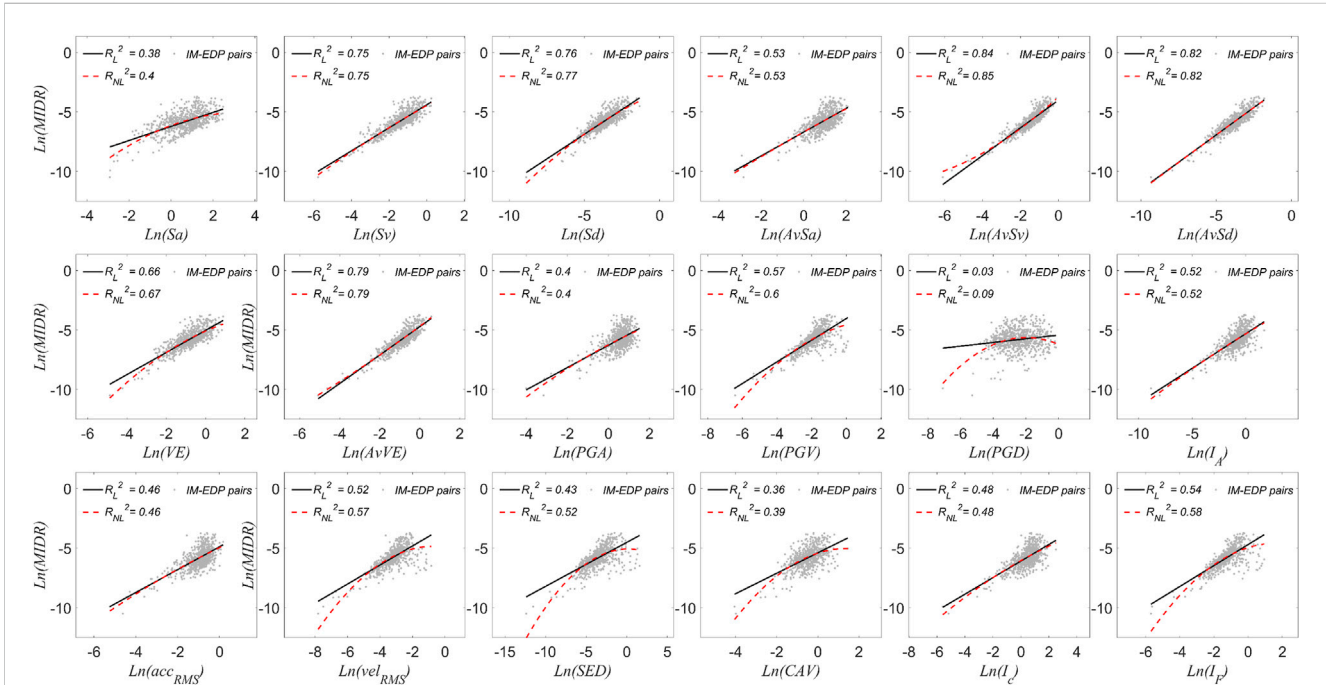

FIGURE 10
IM−EDP pairs using ground motions acting at the base of the buildings.
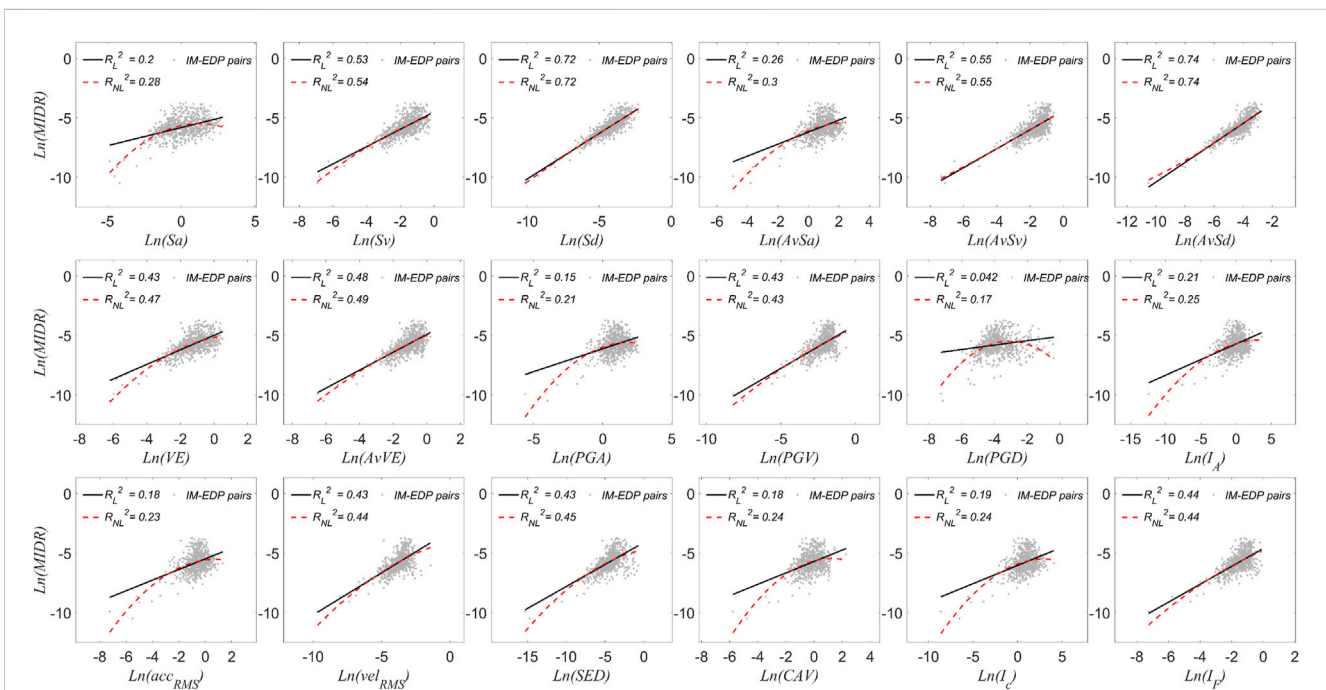
FIGURE 11
IM−EDP pairs using ground motions acting at bedrock level.

consistent with that of the previous research, which has highlighted the capabilities of velocity as an enhanced physical magnitude to predict the deformation field of a structure (Vargas–Alzate et al., 2022b).

7.2.2 Approach 2: IM–EDP pairs using ground motions acting at the bedrock level

Using ground motion records at the surface implies that the effect of seismic wave propagation through the soil is not explicitly considered in the estimation of seismic risk. In this section, the resulting clouds of IM–EDP pairs have been analyzed using the ground motion records acting at the bedrock level. Figure 11 shows the bivariate distribution for IMs and MIDR under the aforementioned condition. As expected, a significant decrease in R^2, for most of the IMs, has been observed.

It can be attributed to the influence of the filtering induced by the soil profile. Notwithstanding, Sd (T_1) and $AvSd$ remain at a significant level of efficiency. This efficiency is not as high as the one observed in the previous approach, where $AvSv$ reached an R^2_{NL} equal to 0.851.

7.2.3 Approach 3: multi-regression model to consider information from soil and ground motion acting at the bedrock level

As previously stated, Eq. 12 allows identifying enhancing arrangements that consider statistical information from several IVs. To do so, it is necessary to replace N_{IV} with the desired number of IVs in this equation. In the present study, $N_{IV} = 2$ and $N_{IV} = 3$ have been tested.

A large set of soil information variables has been included in the identification of the enhanced arrangements. In Table 5, a description of these variables is presented.

For the case of $N_{IV} = 2$, it has been found that $AvSd$ and β_{NL} provide the best fit. Figure 12A shows the bivariate distribution between IM_{GD}–EDP pairs. This arrangement provides an R^2_{NL} equal to 0.794, which is higher than the one exhibited by $AvSd$ in the previous section (0.741). Table 6 shows α values for the 20 most correlated arrangements and the respective information variables (IVs). It can be seen that Sd and $AvSd$ appear in most of the efficient combinations, thus confirming the robustness of spectral displacement IMs with respect to seismic wave propagation. In addition, the standard deviation of the residuals (σ_ε) has also been included for each regression analysis. In this way, in future research, it might be possible not only to perform the best estimate of the EDP but also to take into account the variability of the bivariate distribution in the sampling strategy.

If $N_{IV} = 3$, it has been observed that a mathematical arrangement including $AvSd$, ΔT_{NL}, and $\overline{Vs}_{NL}$ derives the best fit for the bivariate distribution IM_{GD}–EDP. In this case, R^2_{NL} is equal to 0.832, which is very close to the highest efficiency exhibited in the approach 1 by $AvSv$ (Section 7.2.1), thus proving the enhanced capabilities of the multi-regression approach. Table 7 shows the α values for the 20 most correlated arrangements and the respective three IVs. It should be noted that $AvSd$ is present in all the arrangements.

TABLE 5 Description of the soil information variables.

| Variables	Equation	Description
T_{S_L}	$\sum_{i=1}^{nlayer} T_{S_L,i}$	Fundamental period of the soil profile
$T_{S_{NL}}$	$\sum_{i=1}^{nlayer} T_{S_{NL},i}$	Elongated non-linear period of the soil profile
$\bar{\xi}_L$	$\frac{\sum_{i=1}^{nlayer} \xi_{L,i}}{nlayer}$	Average linear damping of the soil profile
$\bar{\xi}_{NL}$	$\frac{\sum_{i=1}^{nlayer} \xi_{NL,i}}{nlayer}$	Average non-linear damping of the soil profile
$\bar{\rho}_S$	$\frac{\sum_{i=1}^{nlayer} \rho_{S,i}}{nlayer}$	Average density of the soil profile
$\overline{Vs}_L$	$\frac{\sum_{i=1}^{nlayer} Vs_{L,i}}{nlayer}$	Average shear wave velocity of the soil profile
$\overline{Vs}_{NL}$	$\frac{\sum_{i=1}^{nlayer} Vs_{NL,i}}{nlayer}$	Average shear wave velocity of the degraded soil profile
ΔT_L	$\lvert T_{S_L} - T_B \rvert$	Absolute difference between the fundamental period of the soil profile and the fundamental period of the building (T_B)
ΔT_{NL}	$\lvert T_{S_{NL}} - T_B \rvert$	Absolute difference between the elongated non-linear period of the soil profile and the fundamental period of the building (T_B)
β_L	$\frac{1}{\lvert 1-(T_{S_L}/T_B)^2 \rvert}$	Dynamic amplification factor considering the fundamental period of the soil profile
β_{NL}	$\frac{1}{\lvert 1-(T_{S_{NL}}/T_B)^2 \rvert}$	Dynamic amplification factor considering the elongated non-linear period of the soil profile
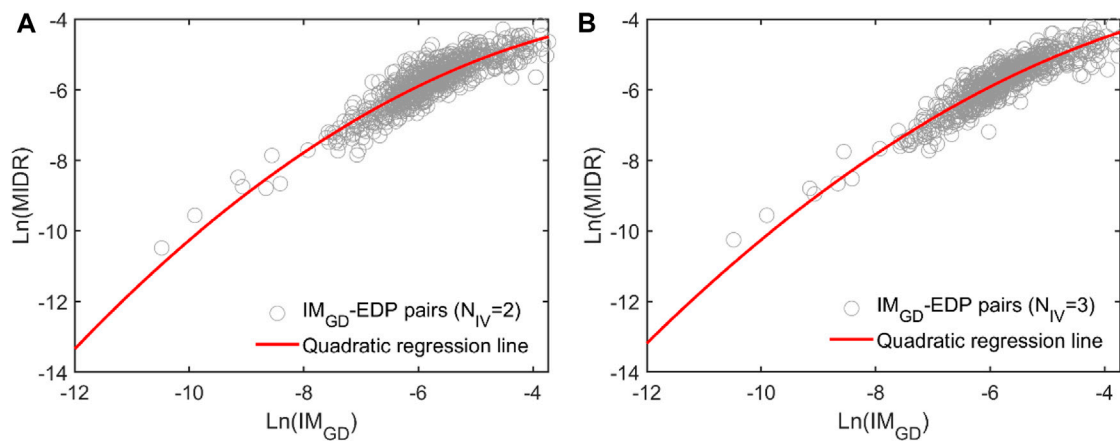
FIGURE 12
(A) IM_{GD}−EDP pairs given N_{IV} =2. **(B)** IM_{GD}−EDP pairs given N_{IV} =3.

TABLE 6 Regression coefficients providing the best fit given N_{IV} =2.

IV_1	IV_2	R^2_{NL}	α_0	α_1	α_2	α_3	α_4	σ_ε
$AvSd$	β_{NL}	0.794	−1.269	1.111	0.027	−0.076	−0.031	0.375
$AvSd$	β_L	0.785	−1.352	1.067	0.025	−0.018	−0.023	0.383
$AvSd$	ΔT_{NL}	0.781	−1.169	1.167	0.030	0.398	−0.316	0.387
Sd	β_{NL}	0.778	−2.174	0.755	−0.002	−0.007	−0.022	0.389
Sa	Sd	0.774	−1.449	−0.205	−0.026	1.041	0.011	0.393
$AvSd$	$T_{S_{NL}}$	0.773	−1.863	1.149	0.028	1.299	−0.582	0.393
Sd	β_L	0.773	−2.245	0.727	−0.004	0.032	−0.018	0.393
$AvSa$	$AvSd$	0.773	−0.389	−0.167	−0.055	1.381	0.044	0.394
$AvSd$	$\bar{\xi}_{NL}$	0.772	−6.085	1.619	0.064	−3.570	−0.498	0.395
$AvSd$	$AvVE$	0.771	0.297	1.903	0.087	−0.638	−0.102	0.395
$AvSd$	vel_{RMS}	0.771	−2.101	1.763	0.079	−1.014	−0.090	0.395
$AvSd$	SED	0.769	−0.482	1.942	0.103	−0.410	−0.030	0.397
$AvSd$	ΔT_L	0.767	−1.344	1.086	0.025	0.129	−0.207	0.399
Sa	$AvSd$	0.766	−0.816	−0.136	−0.017	1.277	0.034	0.399
$AvSd$	$I_{PGV-\Delta}$	0.766	−0.181	1.851	0.092	−0.654	−0.110	0.399
$AvSd$	PGV	0.766	−0.937	1.707	0.075	−0.729	−0.090	0.400
$AvSd$	VE	0.762	−0.416	1.570	0.060	−0.358	−0.052	0.403
Sd	VE	0.761	−0.927	1.486	0.055	−0.549	−0.089	0.404
$AvSd$	T_{S_L}	0.760	−1.902	1.067	0.023	0.963	−0.486	0.405
$AvSv$	$AvSd$	0.758	−0.167	−0.687	−0.099	1.882	0.090	0.407

TABLE 7 Regression coefficients providing the best fit given N_{IV} =3.

IV_1	IV_2	IV_3	R^2_{NL}	α_0	α_1	α_2	α_3	α_4	α_5	α_6	σ_ε
$AvSd$	ΔT_{NL}	$\overline{Vs}_{NL}$	0.832	−11.098	1.363	0.041	−0.036	−0.276	3.352	−0.235	0.339
$AvSd$	ΔT_{NL}	$\bar{\xi}_L$	0.830	−26.096	1.328	0.040	−0.264	−0.386	−8.488	−0.562	0.341
$AvSd$	ΔT_L	$\bar{\xi}_{NL}$	0.826	−4.932	1.774	0.060	−0.014	−0.222	−3.055	−0.331	0.345
$AvSd$	ΔT_{NL}	$\bar{\xi}_{NL}$	0.824	−3.733	1.726	0.057	0.122	−0.239	−2.283	−0.230	0.347
$AvSd$	ΔT_{NL}	$\overline{Vs}_L$	0.823	−14.645	1.244	0.034	−0.010	−0.292	4.411	−0.326	0.347
$AvSd$	ΔT_L	$\overline{Vs}_{NL}$	0.823	−11.389	1.228	0.033	−0.222	−0.225	3.188	−0.209	0.348
$AvSd$	T_{S_L}	$\bar{\xi}_{NL}$	0.818	−5.243	1.792	0.060	0.520	−0.424	−3.132	−0.337	0.352
$AvSd$	β_L	$\bar{\xi}_{NL}$	0.818	−4.969	1.623	0.060	0.090	−0.008	−3.043	−0.391	0.352
$AvSd$	$T_{S_{NL}}$	$\overline{Vs}_{NL}$	0.818	−10.887	1.364	0.041	0.241	−0.376	3.265	−0.227	0.352
$AvSd$	β_{NL}	$\bar{\xi}_{NL}$	0.818	−4.205	1.588	0.057	0.068	−0.011	−2.549	−0.322	0.352
$AvSd$	β_{NL}	$\overline{Vs}_{NL}$	0.818	−10.229	1.173	0.031	0.081	−0.015	3.175	−0.258	0.352
$AvSd$	ΔT_{NL}	T_{S_L}	0.818	−1.042	1.377	0.043	−0.306	−0.504	1.091	0.163	0.353
$AvSd$	β_{NL}	$\bar{\rho}_S$	0.817	−633.116	1.117	0.027	0.017	−0.022	167.214	−11.053	0.353
$AvSd$	$\bar{\xi}_L$	$\overline{Vs}_{NL}$	0.817	−62.719	1.329	0.038	−29.735	−3.869	0.512	0.128	0.354
$AvSd$	$T_{S_{NL}}$	$\bar{\xi}_{NL}$	0.816	−4.002	1.741	0.057	0.484	−0.353	−2.357	−0.237	0.354
$AvSd$	ΔT_{NL}	$\bar{\rho}_S$	0.815	−867.199	1.217	0.033	0.195	−0.299	229.458	−15.185	0.355
$AvSd$	β_L	$\overline{Vs}_{NL}$	0.814	−11.344	1.118	0.027	0.137	−0.008	3.492	−0.283	0.356
$AvSd$	β_{NL}	$\overline{Vs}_L$	0.814	−14.574	1.105	0.027	0.068	−0.018	4.657	−0.393	0.357
$AvSd$	β_L	β_{NL}	0.813	0.027	1.398	0.044	−0.415	0.068	0.448	−0.077	0.357
$AvSd$	$T_{S_{NL}}$	$\bar{\xi}_L$	0.813	−41.214	1.368	0.041	−0.475	−0.393	−15.356	−1.305	0.357

8 Conclusion

In this article, the efficiency prediction of the non-linear dynamic response of reinforced concrete frame structures has been analyzed. The aim has been to develop advanced IMs that consider the dynamic interaction between the building and the underlying soil. The non-linear behavior of the latter has been considered by employing the equivalent linear method (Yoshida et al., 2002). A set of probabilistic soil profiles, structural models, and ground motion records has been used in this research. They have been integrated into a probabilistic framework based on the Monte Carlo method, which allowed the identification of mathematical arrangements highly correlated to the EDP of interest. A 1D model to represent the soil profile has been employed to predict the intensity of ground motions at the surface, once the seismic waves generated by an earthquake reach the base of the building. In doing so, a large group of statistically compatible random soil profiles is generated starting from the main features of a basic set of soil profiles. A database that collects almost 2,000 ground motion records acquired in Colombia has been used to characterize the seismic hazard.

The relationship between IMs and EDPs has been characterized using non-linear regression analysis in the log–log space. In this respect, the linear least squares model allows for different types of regression, and it can be used to extract statistical information from IM–EDP pairs. In general, a polynomial regression model has been used to quantify the efficiency of these pairs, where the higher the coefficient of determination, R^2, the lower the variability in seismic risk estimates. It allowed identifying the most efficient IMs, given specific approaches.

First, the causal relationship between IMs acting at the base of the structural models and the MIDR has been analyzed. From these results, it has been observed that $AvSv$ is the most efficient IM to predict this EDP. This is consistent with previous observations performed in Vargas–Alzate et al., 2022b. The second approach has been applied to identify the most efficient IM to predict the same EDP, but, in this case, IMs have been extracted from the ground motions acting at the bedrock level. As a consequence, two main conclusions have been drawn: i) the efficiency to predict the EDP significantly decreased, and ii) the most efficient IM has been $AvSd$. In fact, it has been observed that the IMs extracted from the displacement spectra [Sd (T$_1$) and $AvSd$] are least likely to lose efficiency when the soil–structure interaction model is employed. The third approach has been to develop a mathematical arrangement with increased efficiency, called IM$_{GD}$, that extracts information not only from the acting ground motion at the bedrock level but also from the dynamic properties of the soil. In this approach, two cases have been explored. First, the most efficient pair of IVs providing the best fit has been found. This significantly increased the efficiency, although it was not as close to the maximum correlation provided by the first approach, where $AvSv$ exhibited an R^2_{NL} equal to 0.855. Thus, the

second approach has been oriented to look for the slate of three ($N_{IV} = 3$) IVs that provide the best fit. An R^2_{NL} equal to 0.832 has been achieved. In this case, the resulting equation depended on $AvSd$, the elongated period of the soil profile, and the degraded shear-wave velocity average. This indicates that the probabilistic framework properly reflects the resonance effect since the mathematical arrangement identified as the most efficient one (IM_{GD}) includes a variable related to the proximity between the fundamental period of the structure and the soil. In addition, several arrangements exhibiting high levels of efficiency have been presented for the cases $N_{IV} = 2$ and $N_{IV} = 3$. In this way, it may be possible in future research to have an estimate of the EDP under study, by considering different types of information. In addition, information regarding the statistical variability of the bivariate distribution has also been provided.

Future research should be oriented toward extending the computational framework to 3D soil models. Moreover, multi-regression models can also be used to develop vector-valued (Baker, 2007) IMs, which generally increase the efficiency of predicting EDPs (Vargas-Alzate et al., 2022a). It is also important to analyze how efficiency behaves when analyzing results classified according to the number of storeys. Preliminary results indicate that these sub-classifications tend to increase efficiency. It is worth mentioning that the results presented in this research are tied to the soil type studied. Therefore, a correct parametrization of the degradation curves (see Figure 8) is a key aspect of the presented framework. In general, the analysis of new soil configurations, EDPs, IMs, and structural typologies will also provide valuable information to enhance the capabilities of the proposed model.

Data availability statement

The raw data supporting the conclusion of this article will be made available by the authors, without undue reservation.

Author contributions

Conceptualization, AZ-F and YV-A. Methodology, AZ-F, YV-A, and LP. Software, AZ-F and YV-A. Writing—original draft preparation, AZ-F and YV-A. Writing—review and editing, AZ-F, YV-A, LP, and RG-D. Visualization, AZ-F, YV-A, LP, and RG-D. All authors contributed to the article and approved the submitted version.

Funding

Conflict of interest

The authors declare that the research was conducted in the absence of any commercial or financial relationships that could be construed as a potential conflict of interest.

Publisher's note

All claims expressed in this article are solely those of the authors and do not necessarily represent those of their affiliated organizations, or those of the publisher, the editors, and the reviewers. Any product that may be evaluated in this article, or claim that may be made by its manufacturer, is not guaranteed or endorsed by the publisher.

References

Angelini, M. E., and Heuvelink, G. B. M. (2018). Including spatial correlation in structural equation modelling of soil properties. *Spat. Stat.* 25, 35–51. doi:10.1016/j.spasta.2018.04.003

Arias, A. (1970). "Measure of earthquake intensity," in *Seismic design for nuclear power plants*. Editors Hansen and J. Robert (Cambridge: Massachusetts Inst. of Tech. Press), 438–483.

Baker, J. W. (2007). Probabilistic structural response assessment using vector-valued intensity measures. *Earthq. Eng. Struct. Dyn.* 36, 1861–1883. doi:10.1002/eqe.700

Beck, J. L., and Hall, J. F. (1986). Factors contributing to the catastrophe in Mexico City during the earthquake of September 19, 1985. *Geophys Res. Lett.* 13, 593–596. doi:10.1029/GL013i006p00593

Benavent-Climent, A., Akiyama, H., López-Almansa, F., and Pujades, L. G. (2004). Prediction of ultimate earthquake resistance of gravity-load designed RC buildings. *Eng. Struct.* 26, 1103–1113. doi:10.1016/j.engstruct.2004.03.011

Bommer, J. J., and Acevedo, A. B. (2004). The use of real earthquake accelerograms as input to dynamic analysis. *J. Earthq. Eng.* 8, 43–91. doi:10.1080/13632460409350521

Carr, J. (2007). Ruaumoko-inelastic dynamic analysis program. Version.

Carrière, S. R., Jongmans, D., Chambon, G., Bièvre, G., Lanson, B., Bertello, L., et al. (2018). Rheological properties of clayey soils originating from flow-like landslides. *Landslides* 15, 1615–1630. doi:10.1007/s10346-018-0972-6

Chapra, S. C. (2018). *Applied numerical methods with MATLAB® for engineers and scientists*. New York, NY: McGraw-Hill Education.

Cheng, Y., Lucchini, A., and Mollaioli, F. (2015). Correlation of elastic input energy equivalent velocity spectral values. *Earthquakes Struct.* 8, 957–976. doi:10.12989/eas.2015.8.5.957

Comartin, C. D., Niewiarowski, R. W., Freeman, S. A., and Turner, F. M. (2000). Seismic evaluation and retrofit of concrete buildings: A practical overview of the atc 40 document. *Earthq. Spectra* 16, 241–261. doi:10.1193/1.1586093

Cruz, C., and Miranda, E. (2021). Insights into damping ratios in buildings. *Earthq. Eng. Struct. Dyn.* 50, 916–934. doi:10.1002/eqe.3356

Eads, L., Miranda, E., and Lignos, D. G. (2015). Average spectral acceleration as an intensity measure for collapse risk assessment. *Earthq. Eng. Struct. Dyn.* 44, 2057–2073. doi:10.1002/eqe.2575

Fajfar, P., Vidic, T., and Fischinger, M. (1990). A measure of earthquake motion capacity to damage medium-period structures. *Soil Dyn. Earthq. Eng.* 9, 236–242. doi:10.1016/S0267-7261(05)80002-8

Fiorentino, G., Quaranta, G., Mylonakis, G., Lavorato, D., Pagliaroli, A., Carlucci, G., et al. (2019). Seismic reassessment of the leaning tower of pisa: Dynamic monitoring, site response, and SSI. *Earthq. Spectra* 35, 703–736. doi:10.1193/021518EQS037M

FOPAE (2011). Procesamiento e interpretación de señales de la red de acelerógrafos de Bogotá 2009 - 2011. *IDIGER*. Bogotá.

Grigoriu, M. (2016). Do seismic intensity measures (IMs) measure up. *undefined* 46, 80–93. doi:10.1016/J.PROBENGMECH.2016.09.002

Güllü, A., Yüksel, E., Yalçın, C., Anıl Dindar, A., Özkaynak, H., and Büyüköztürk, O. (2019). An improved input energy spectrum verified by the shake table tests. *Earthq. Eng. Struct. Dyn.* 48, 27–45. doi:10.1002/eqe.3121

Hardin, B. O., and Scott, G. D. (1967). Generalized Kelvin-Voigt used in soil dynamics study. *J. Eng. Mech. Division* 93, 79–79. doi:10.1061/JMCEA3.0000830

Haselton, C. B., Atkinson, S., Jonathan, H. A., and Grant, N. (2012). "Selecting and scaling earthquake ground motions for performing response-history analyses," in *15th world conference on earthquake engineering* (Lisboa, Portugal: NIST GCR).

Housner, G. W. (1975). "Measures of severity of earthquake ground shaking," in *Proc. US natl. Conf. Earthq. Eng. Earthquake Engineering Research Institute* (Ann Arbor Michigan).

Jalayer, F., De Risi, R., and Manfredi, G. (2015). Bayesian Cloud Analysis: Efficient structural fragility assessment using linear regression. *Bull. Earthq. Eng.* 13, 1183–1203. doi:10.1007/S10518-014-9692-Z

Kaklamanos, J., Baise, L. G., Thompson, E. M., and Dorfmann, L. (2015). Comparison of 1D linear, equivalent-linear, and nonlinear site response models at six KiK-net validation sites. *Soil Dyn. Earthq. Eng.* 69, 207–219. doi:10.1016/j.soildyn.2014.10.016

Kazantzi, A. K., and Vamvatsikos, D. (2015). Intensity measure selection for vulnerability studies of building classes. *Earthq. Eng. Struct. Dyn.* 44, 2677–2694. doi:10.1002/EQE.2603

Kohrangi, M., Bazzurro, P., Vamvatsikos, D., and Spillatura, A. (2017). Conditional spectrum-based ground motion record selection using average spectral acceleration. *Earthq. Eng. Struct. Dyn.* 46, 1667–1685. doi:10.1002/EQE.2876

Kostinakis, K., Fontara, I. K., and Athanatopoulou, A. M. (2018). Scalar structure-specific ground motion intensity measures for assessing the seismic performance of structures: A review. *J. Earthq. Eng.* 22, 630–665. doi:10.1080/13632469.2016.1264323

Krinitzsky, E. L. (2003). How to combine deterministic and probabilistic methods for assessing earthquake hazards. *Eng. Geol.* 70, 157–163. doi:10.1016/S0013-7952(02)00269-7

Kroese, D. P., and Rubinstein, R. Y. (2012). Monte Carlo methods. *Wiley Interdiscip. Rev. Comput. Stat.* 4, 48–58. doi:10.1002/wics.194

Kucherenko, S., Albrecht, D., and Saltelli, A. (2015). Exploring multi-dimensional spaces: A comparison of Latin hypercube and quasi Monte Carlo sampling techniques. arXiv.

Kumar, A., and Mondal, J. K. (2017). Newly developed MATLAB based code for equivalent linear site response analysis. *Geotechnical Geol. Eng.* 35, 2303–2325. doi:10.1007/s10706-017-0246-4

Lou, M., Wang, H., Chen, X., and Zhai, Y. (2011). Structure–soil–structure interaction: Literature review. *Soil Dyn. Earthq. Eng.* 31, 1724–1731. doi:10.1016/j.soildyn.2011.07.008

Luco, N., and Cornell, C. A. (2019). Structure-specific scalar intensity measures for near-source and ordinary earthquake ground motions. *Sage Journals* 23, 357–392. doi:10.1193/1.2723158

Mayes, R. L. (1995). Interstory drift design and damage control issues. *Struct. Des. Tall Build.* 4, 15–25. doi:10.1002/tal.4320040104

Nakamura, Y. (1989). A method for dynamic characteristics estimation of subsurface using microtremor on the ground surface. *Railw. Tech. Res. Institute/Tetsudo Gijutsu Kenkyujo* 30, 25–33.

Ohnaka, M. (1976). A physical basis for earthquakes based on the elastic rebound model. *Bull. Seismol. Soc. Am.* 66, 433–451. doi:10.1785/BSSA0660020433

Okur, D. V., and Ansal, A. (2007). Stiffness degradation of natural fine grained soils during cyclic loading. *Soil Dyn. Earthq. Eng.* 27, 843–854. doi:10.1016/j.soildyn.2007.01.005

Pagliaroli, A., Lanzo, G., Tommasi, P., and Di Fiore, V. (2014). Dynamic characterization of soils and soft rocks of the central archeological area of rome. *Bull. Earthq. Eng.* 12, 1365–1381. doi:10.1007/s10518-013-9452-5

Park, R., and Paulay, T. (1991). *Reinforced concrete structures*. New York, NY: John Wiley and Sons. Available at: https://books.google.es/books?id=QPDvchXv5zUC.

Park, Y. J., Ang, A. H. S., and Wen, Y. K. (1987). Damage-limiting aseismic design of buildings. *Earthq. Spectra* 3, 1–26. doi:10.1193/1.1585416

Pejovic, J., and Jankovic, S. (2015). Selection of ground motion intensity measure for reinforced concrete structure. *Procedia Eng.* 117, 588–595. doi:10.1016/j.proeng.2015.08.219

Pinzón, L. A., Vargas-Alzate, Y. F., Pujades, L. G., and Diaz, S. A. (2020). A drift-correlated ground motion intensity measure: Application to steel frame buildings. *Soil Dyn. Earthq. Eng.* 132, 106096. doi:10.1016/j.soildyn.2020.106096

Pitilakis, D., and Petridis, C. (2022). Fragility curves for existing reinforced concrete buildings, including soil–structure interaction and site amplification effects. *Eng. Struct.* 269, 114733. doi:10.1016/j.engstruct.2022.114733

Pitilakis, D. (2023). Waveprop. Available at: https://www.mathworks.com/matlabcentral/fileexchange/60589-waveprop.

Reed, J. W., and Kassawara, R. P. (1990). A criterion for determining exceedance of the operating basis earthquake. *Nucl. Eng. Des.* 123, 387–396. doi:10.1016/0029-5493(90)90259-Z

Sarma, S. K. (1971). Energy flux of strong earthquakes. *Tectonophysics* 11, 159–173. doi:10.1016/0040-1951(71)90028-X

Sarma, S. K., and Yang, K. S. (1987). An evaluation of strong motion records and a new parameterA95. *Earthq. Eng. Struct. Dyn.* 15, 119–132. doi:10.1002/eqe.4290150109

SGC (2020). Sistema de Consulta de la Amenaza Sísmica de Colombia. Available at: https://amenazasismica.sgc.gov.co/.

Shedlock, K. M. (2002). "Global seismic hazards," in *Encyclopedia of physical science and technology* (Elsevier), 825–832. U.S. Geological Survey, Denver, Colorado, USA. doi:10.1016/B0-12-227410-5/00295-7

Silva, W. J., Abrahamson, N., Toro, G., and Constantino, C. (1996). *Description and validation of the stochastic ground motion model.* California: Pacific Engineering and Analysis.

Toro, G. R. (2022). Uncertainty in shear-wave velocity profiles. *J. Seismol.* 26, 713–730. doi:10.1007/s10950-022-10084-x

Tothong, P., and Luco, N. (2007). Probabilistic seismic demand analysis using advanced ground motion intensity measures. *Earthq. Eng. Struct. Dyn.* 36, 1837–1860. doi:10.1002/eqe.696

Vanmarcke, E. H. (1977). Probabilistic modeling of soil profiles. *J. Geotechnical Eng. Div.* 103, 1227–1246. doi:10.1061/AJGEB6.0000517

Vargas Alzate, Y. F., Pujades Beneit, L. G., Barbat, A. H., Hurtado Gomez, J. E., Diaz Alvarado, S. A., and Hidalgo Leiva, D. A. (2018). Probabilistic seismic damage assessment of reinforced concrete buildings considering directionality effects. *Struct. Infrastructure Eng.* 14, 817–829. doi:10.1080/15732479.2017.1385089

Vargas-Alzate, Y. F., Gonzalez-Drigo, R., and Avila-Haro, J. A. (2022a). Multi-regression analysis to enhance the predictability of the seismic response of buildings. *Infrastructures (Basel)* 7, 51. doi:10.3390/infrastructures7040051

Vargas-Alzate, Y. F., Hurtado, J. E., and Pujades, L. G. (2022b). New insights into the relationship between seismic intensity measures and nonlinear structural response. *Bull. Earthq. Eng.* 20, 2329–2365. doi:10.1007/s10518-021-01283-x

Wesnousky, S. G. (1994). The Gutenberg-Richter or characteristic earthquake distribution, which is it? *Bull. Seismol. Soc. Am.* 84, 1940–1959. doi:10.1785/BSSA0840061940

Yazgan, U. (2012). Proposal of energy spectra for earthquake resistant design based on Turkish registers. Available at: https://dialnet.unirioja.es/servlet/tesis?codigo=95317.

Yoshida, N., Kobayashi, S., Suetomi, I., and Miura, K. (2002). Equivalent linear method considering frequency dependent characteristics of stiffness and damping. *Soil Dyn. Earthq. Eng.* 22, 205–222. doi:10.1016/S0267-7261(02)00011-8